Synthesis and characterization of -MoO_3 microspheres packed with nanoflakes

2014 J. Phys. D: Appl. Phys. 47 065305

(http://iopscience.iop.org/0022-3727/47/6/065305)

IOP Publishing Journal of Physics D: Applied Physics

J. Phys. D: Appl. Phys. **47** (2014) 065305 (9pp) doi:10.1088/0022-3727/47/6/065305

Synthesis and characterization of α-MoO_3 microspheres packed with nanoflakes

Rabindar K Sharma and G B Reddy

Thin Film Laboratory, Department of Physics, Indian Institute of Technology Delhi, New Delhi (India)–110016, India

E-mail: rkrksharma6@gmail.com

Received 20 September 2013, revised 2 December 2013
Accepted for publication 4 December 2013
Published 15 January 2014

Abstract

In this paper, we report the fabrication of three-dimensional molybdenum oxide (α-MoO_3) microspheres (MSs) packed with nanoflakes by facile and eco-friendly physical vapour deposition processes. Synthesis processes include sequences of plasma-assisted sublimation and thermal evaporation routes on a nickel-coated glass substrate in three individual stages. It is observed that nanostructured films deposited in the first and second stages function as seed layers for the growth of MoO_3 MSs. The structural study divulged that the MoO_3 MSs are polycrystalline in nature with pure orthorhombic phase. The morphological study endorses the uniform growth of MSs on a large area scale having diameters in the range of 0.7–2 μm with the finely packed single crystalline nanoflakes with mean thicknesses of nearly 60 nm. These single crystalline flakes are not individual but in the form of randomly distributed bunches embedded on the surface of MSs. Vibrational study of molybdenum and oxygen atoms in the MSs is carried out by Raman and Fourier transform infrared analysis, which further assured the existence of a pure orthorhombic crystal phase of MoO_3 MSs and also justified the x-ray diffractogram findings. The MoO_3 MSs show intense photoluminescence emission at room temperature with the five prominent peaks located at 424, 457, 486, 521 and 536 nm in accordance with the improvement in the degree of crystallinity. The possible growth strategy of α-MoO_3 MSs packed with nanoflakes is proposed in this paper briefly.

Keywords: microspheres (MSs), nanoflakes, plasma-assisted sublimation process, thermal evaporation

(Some figures may appear in colour only in the online journal)

1. Introduction

Over the past several years, the synthesis of three-dimensional hierarchical inorganic micro/nanomaterials, ordinarily nanoparticles (0D) [1], nanorods (1D) [2], nanoplates (2D) [3] as building blocks, have aroused extensive attention owing to their wide spread application in catalysis, lithium ion batteries, and water treatment [4–6] etc. Nowadays, research focused on nanomaterials has rapidly extended into controlling the shape of materials and understanding the correlations between the material properties and their nanostructures and morphology. Being a smart functional material, molybdenum oxide (MoO_3) is one of the important wide band gap semiconducting materials with promising applications in low-cost electrochromic devices, [7] gas sensors [8] and field emitters [9], as well as in electrodes in lithium ion batteries. The properties of MoO_3 nanostructures depend highly on their shapes, sizes, aspect ratio, orientations and crystalline density. A variety of MoO_3 nanostructures, such as nanowires, nanotubes, nanobelts, nanostars, nanorods, nanoflakes and nanospheres, have been prepared by different routes. Zhou *et al* [10] grew α-MoO_3 nanowires using a thermal evaporation (TE) method under vacuum conditions at a very high boat temperature of 1100 °C on silicon substrates. Diaz-Droguett *et al* [11] synthesized a variety of molybdenum trioxide nanostructures, such as nanoribbons, nanofibres, nanoniddles and nanoparticles, by the direct TE of MoO_3 powder at high temperatures. Yan *et al* [12] reported the growth of α-MoO_3 nanoflakes on an Au-coated silicon substrate using a modified hot plate method at a temperature

of 450 °C. Khademi *et al* [13] synthesized MoO_3 nanostars by TE. Zakharova *et al* [14] fabricated $MoO_{3-\delta}$ nanorods by the hydrothermal process of molybdic acid and studied their magnetic properties. Song *et al* [15] successfully synthesized MoO_3 nanofibres/nanobelts using the surfactant templated hydrothermal process. Liu *et al* [16] demonstrated the growth of hollow nanospheres of MoO_3 and WO_3 assembled with the polymeric micelles by using a soft template of polymeric micelle with the core–shell–corona architecture. Taking this into account, micro/nanometre sized hierarchical metal oxides offer very large surface areas, are the most suitable candidates for novel device application, and few reports based on the synthesis of hierarchical architectures of metal oxides have been demonstrated with their applications. For example, Fei *et al* [17] synthesized micrometre-scale manganese oxide hierarchical hollow nanostructures, which displayed good abilities in removing water contamination. Lin *et al* [5] reported the growth of $CoMn_2O_4$hierarchical microspheres (MSs) assembled with porous nanosheets as stable anodes for lithium ion batteries. The importance of hierarchical microstructures of metal oxides in various applications prompted us to carry out the present work. Among the various morphological structures mentioned above, MSs—especially those with a uniform size and shape—have attracted much attention because of their large specific area and mechanical and thermal stabilities. Although dense MoO_3 nanoparticles and the hollow nanospheres are reported so far, no MSs of MoO_3 packed with the vertically aligned nanoflakes by the simple and low-cost physical vapour deposition (PVD) process have been reported. In particular, most research groups have employed chemical routes to prepare complex hierarchical micro-/nanomaterials rather than a PVD process, like a simple electrochemical route [18], biomolecule-assisted solution approach [19] and hydrothermal synthesis [20] etc. Even though chemical routes do work, they have some limitations. For instance, chemical routes are complex, more or less produce contamination, and need several steps of washing, purification and drying etc. Thus, from a technical point of view, developing convenient and effective pathways for the synthesis of a novel template and surfactant-free hierarchical structures is of special significance and becomes an intensive research topic.

Herein, we report a remarkably simple and eco-friendly PVD route for the controlled growth of α-MoO_3 micro-scale spheres packed with the self-assembled bunches of vertically aligned nanoflakes on a large area of a nickel-coated glass substrate without any templates or surfactants. The deposition process includes both the plasma-assisted sublimation (PAS) and TE process in three consecutive steps. Surface morphological, structural, optical and vibrational study, as well as the possible growth mechanism of the finally obtained MoO_3 MSs, are discussed in this paper. Studies concerning morphological, structural and optical properties of MoO_3 MSs are investigated systematically by scanning electron microscope (SEM), transmission electron microscope (TEM), x- diffractogram (XRD) and photoluminescence (PL) spectroscopy. The detailed morphological study of MSs further carried out by a high resolution transmission electron microscope (HRTEM) with selected area electron diffraction (SAED). Both the Raman and Fourier transform infrared (FTIR) spectroscopes are employed to study the vibrational properties of MoO_3 MSs. All observed results are in good agreement with each other.

2. Experimental details

Multilayered molybdenum oxide thin films were deposited alternately in three steps on the nickel-coated glass substrate using the PAS and TE processes. In the first deposition step, the MoO_3 film is deposited on the Ni-coated glass substrate using the PAS process, the second step includes the deposition of MoO_3 on the pre-deposited substrate by TE at room temperature and the third/last step incorporates MoO_3 film deposition by the same process as used in the first step. Initially the nickel film with a thickness of about 100 nm was deposited on the glass substrate by thermally evaporating (99.99% Aldrich) pure nickel powder at base vacuum of 7.5×10^{-6} Torr. Ni-coated glass is used as the substrate in this growth process. In the PAS process, during the first step, the Ni-coated glass substrate is mounted on a Mo strip (taken as a sublimation source) and the sublimation source temperature is gradually increased up to 500 °C by suitably adjusting the current across it. For the uniform deposition to occur on a large scale, the optimum ratio of the substrate area to that of the Mo strip $(8 \times 3)\,cm^2$ was nearly 1/8. Both the sublimation source (Mo strip) as well as the substrate is located between electrodes in such a manner that they get exposed entirely to oxygen plasma. Before switching plasma, the chamber was evacuated to attain the base vacuum of the order of 7.5×10^{-6} Torr. After that 99.9% of pure oxygen was pursed in the chamber to maintain the constant chamber pressure in the range of 7.5×10^{-2} Torr and stable plasma is created between the electrodes, placed at an optimum separation of 7.5 cm by applying the potential difference of 2500 V between the electrodes. In the second step, the molybdenum oxide film is deposited on the pre-deposited film by TE of MoO_3 powder (Merck 99.99%) at a base vacuum of 7.5×10^{-6} Torr at room temperature without oxygen plasma ambience. The last deposition step further includes the PAS process to deposit the MoO_3 film under the same processing parameters as in the first step. In each step, the deposition duration is fixed as 1/2 hr. The surface microstructures of films after every deposition step are studied with SEM (ZEISS EVO Series SEM model EVO-50). To record the surface topography with SEM, the samples were mounted on a holder and a thin layer of gold was deposited to avoid charging due to the probing electron beam. Structural analysis of the MoO_3 MSs was carried out with a Philips x-ray diffractometer, using Cu K_α radiation ($\lambda \sim 1.54$ Å) with the glancing angle kept constant at 1°. The XRDs were recorded in the 2θ range of 10°–60° and the x-rays generated were used with an electron beam current of 40 mA and accelerating voltage of 45 kV. The step size was 0.5° and dwell time at each step was 0.05 s. The average crystallite size of the samples is calculated theoretically using the following Debye–Scherrer equation:

$$D_{hkl} = \frac{k\lambda}{\beta\,(h\,k\,l)\cdot\cos(\theta_{hkl})}$$

Table 1. Details of all five samples used in this work with their abbreviations.

	Sample name	Sample details
1.	T	Deposition of Ni film on glass substrates (acting as a substrate in all cases).
2.	S	MoO_3 film deposited on the Ni-coated glass substrate by the PAS) process at 500 °C.
3.	S–T	Deposition of MoO_3 film by the PAS process on the thermally evaporated MoO_3 thin film.
4.	T–S	Deposition of MoO_3 film by the TE process on the MoO_3 thin film deposited by PAS process.
5.	S–T–S	Deposition of MoO_3 by the PAS process + deposition of MoO_3 by TE process + Again the deposition of MoO_3 by the PAS process on the same substrate.

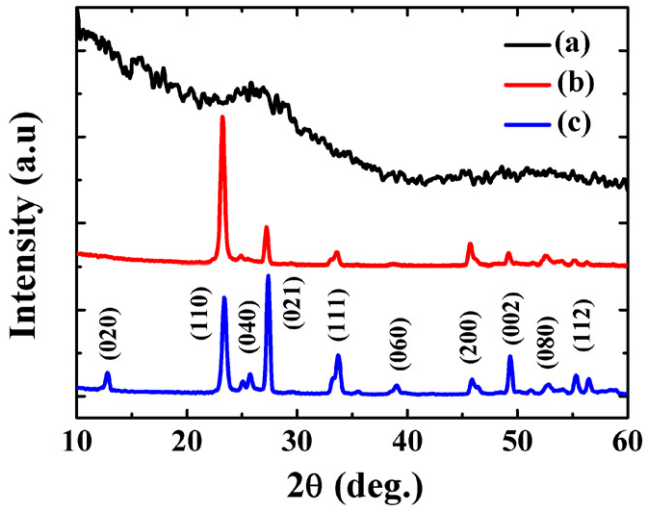

Figure 1. XRD pattern of orthorhombic MoO_3 nanostructured thin films (matched according to JCPDS Ref. Code: 00-005-508): (*a*) deposited on the glass substrate by TE at room temperature. (*b*) The case of samples (S–T) after the second deposition step (*c*) of sample (S–T–S) after the final deposition step.

where $D_{h\,k\,l}$ is the average linear dimension of the crystal perpendicular to the diffracting plane $(h\,k\,l)$, λ is the wavelength of the incident x-ray beam, $\theta_{h\,k\,l}$ is the Bragg angle, k is the shape factor with a value in vicinity of 1 and β $(h\,k\,l)$ is the full-width at half-maximum (FWHM) in radians of the most intense diffraction peaks corrected for the instrumental line broadening. Vibrational study of MSs was carried out by micro-Raman spectroscopy of Renishaw inVia (excited with an Ar^+ line at 514.5 nm) and Perkin Elmer (Spectrum BX) FTIR in the spectral ranges 200–1000 cm^{-1} and 400–1500 cm^{-1}, respectively, with resolutions of 1 and 4 cm^{-1} TEM studies of MSs are carried out on Philips Model CM12 operated at 120 kV with SAED analysis. The specimens for TEM measurement were prepared by suspending the deposited films in ethanol and placing some droplets of this solution onto the standard carbon supported 600 mesh copper grid and drying them slowly. More insightful characterization is performed on HRTEM. A Horiba Jobin Yvon spectroflourometer (Flurolog III), taking a 450 W xenon lamp as the source and a R928P photomultiplier tube in photo-counting mode as the detector, is employed for PL measurements. The thickness of films in each deposition step is determined by an AMBIOS Technology (XP-2) Stylus profilometer. All measurements are performed at room temperature. In this work all investigations are carried out on five different samples and their corresponding details with their abbreviations are given in table 1.

3. Result and discussion

XRDs of T, S–T and S–T–S samples are shown in figures 1(*a*)–(*c*). Initially an amorphous nickel film is deposited on the bare glass substrate using the TE process, this nickel-coated glass acts as a substrate in all cases. The absence of diffraction peaks in the XRD pattern of MoO_3 deposited on nickel-coated glass by the TE process (sample T) confirms its amorphous nature shown in figure 1(*a*), whereas the diffractogram of the MoO_3 nanostructured thin film deposited on the Ni-coated glass substrate at 500 °C using the PAS process (sample S) is exhibited in figure 1(*b*), and the observed sharp and well intense peaks correspond to the pure orthorhombic phase. Interestingly, the diffraction peak corresponding to the (1 1 0) crystal plane showed the strongest intensity, which endorsed the fact that the grown structure tends to be preferentially oriented along the [1 1 0] crystallographic direction. No trace of the other phase and impurities was detected within the detection limit of x-ray diffraction, revealing that the film in sample S shows a pure orthorhombic phase after the first deposition step. No phase change is recorded in the case of sample (T–S) after the second deposition step. The XRD pattern of the finally grown structure (MSs packed with vertically aligned nanoflakes) in sample (S–T–S) also exhibits a single orthorhombic phase without any impurity, the same as previously, as can be seen in figure 1(*c*). The obtained average values for the lattice parameters are $a = 3.85$ Å, $b = 13.849$ Å and $c = 3.691$ Å, which are in good agreement with the reported values given in the Joint Committee on Powder Diffraction Standards (JCPDS) (Ref. Code: 00-005-508) ($a = 3.962$ Å, $b = 13.858$ Å and $c = 3.697$ Å) for α-MoO_3 MSs. High intensity and broad spectral width of the peaks in the diffractogram of the S–T–S sample asserts that the grain size calculated by the Debye–Scherrer formula [21] is approximately 45 nm whereas the grain size in the case of sample S–T is smaller, 39.8 nm, than previously, which assured an improvement in the degree of crystallinity. It is worthwhile to note that the intensity of the peaks observed from most of the crystal planes in S–T–S is substantial, which clearly revealed the random alignment of grown nanostructures during the final deposition stage.

The modification in surface morphology of MoO_3 thin films is captured after every deposition step by SEM to understand the growth of MSs systematically. The recorded SEM micrographs of S, T–S, S–T and S–T–S samples are shown in figures 2 and 3. Initially, the nickel film deposited on the bare glass substrate using the TE process at room temperature shows the completely smooth surface, as can be seen in figure 2(*a*). In the first deposition step, vertically aligned nanoflakes with very high aspect ratios (>20) and

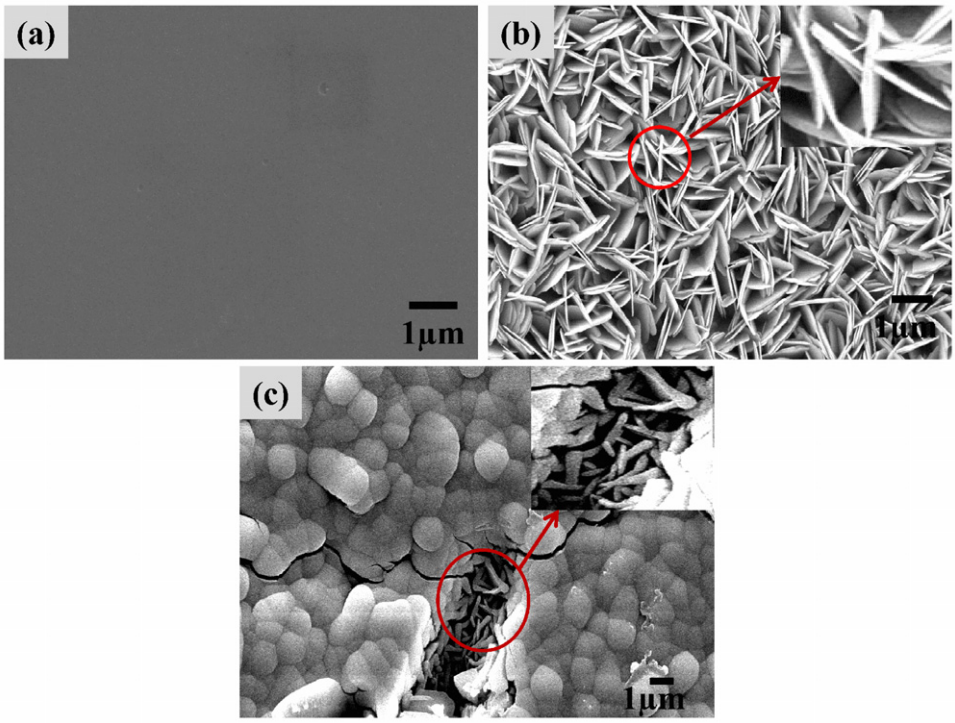

Figure 2. SEM micrographs of: (*a*) as deposited Ni films. (*b*) Nanoflakes grown during the first growth step (sample S). (*c*) MoO_3 film deposited on nanoflakes by TE with the inset image confirming the formation of canopies with spherical contours (sample T–S).

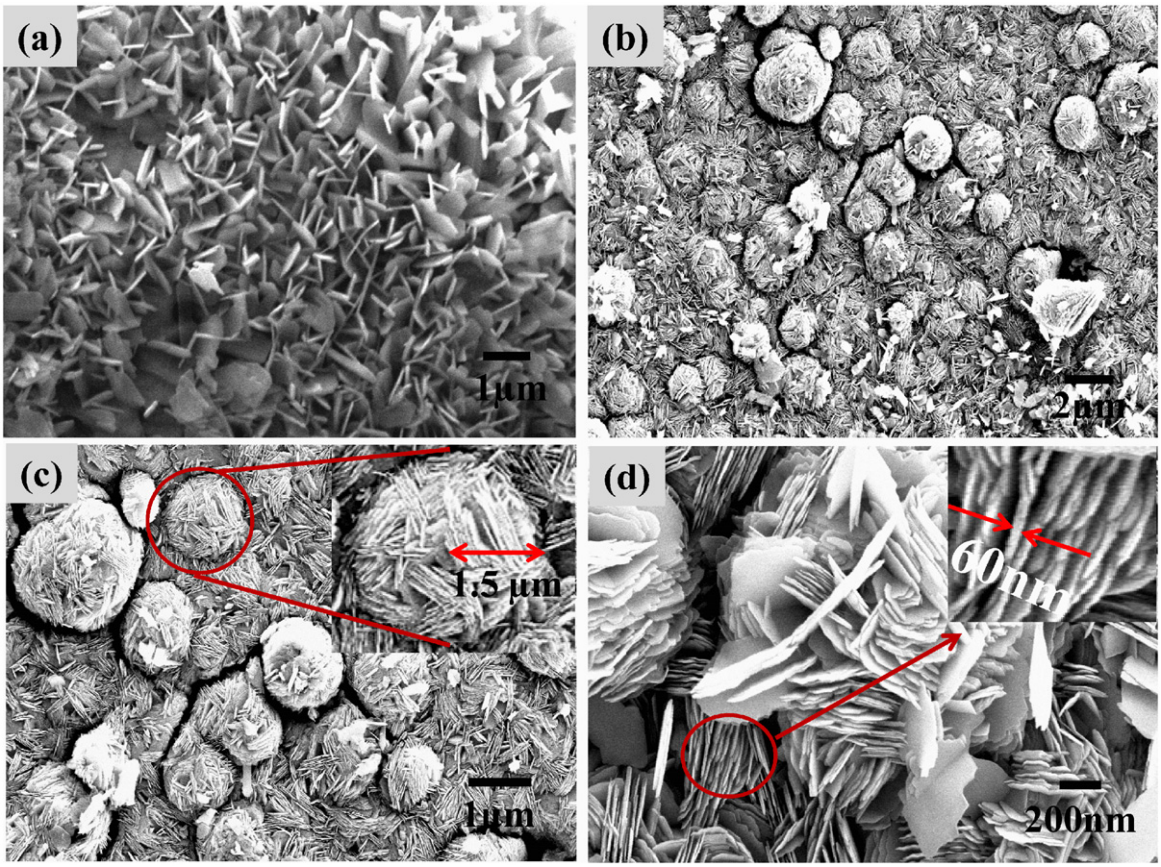

Figure 3. SEM micrographs: (*a*) sample T–S shows the formation of MoO_3 nanoplates rather than MSs; (*b*) surface microstructure of MSs at low magnification (5 K); (*c*) surface structure of MSs at higher magnification with the typical radius highlighted in the inset (10 K); (d) MoO_3 MSs with nanoflakes assembled in parallel on their surface (20 K).

mean heights of nearly 1.5 μm (sample S) are formed by the PAS process. As reported earlier [22], the shape orientation of nanosize features strongly depends on the deposition conditions namely sublimation source temperature, deposition duration and plasma parameters etc. In the present study, the optimized parameters are used to obtain vertically aligned nanoflakes, as can be seen in figure 2(*b*). After the second deposition step, the obtained surface morphology of the film in the T–S sample is strongly determined by the bottom layer, deposited by the PAS process in the first step. The formation of canopies with spherical contours covering the nanoflakes is observed (see figure 2(*c*)). These contours on the canopies are guided by the variation in the heights of nanoflakes on the bottom layer. The accidental rupture in the top layer shows that the vertical flakes of the bottom layer are intact, which confirms the formation of nearly spherical contours on the top layer. The inset of figure 2(*c*) shows the surface morphology of both the consecutive films layer-by-layer. In the second step, since thermal deposition is carried out at room temperature, which leads to the incoming MoO_3 adatoms having less mobility when reaching the substrate, also promotes the formation of canopies with spherical contours like morphology. These spherical contours act as a core of MSs. The low magnification SEM micrographs of the S–T–S sample, as shown in figure 3(*b*)–(*c*), demonstrate the formation of MoO_3 MSs packed with nanoflakes, but are non-uniform as a function of radius. The surface morphology is quite uniform, confirming the growth process is progressed uniformly on the entire substrate over the large substrate area (15×20) mm^2. The obtained MoO_3 MSs have diameters lying in the range 0.7–3 μm. The MS with a typical diameter of 1.5 μm is shown in the inset of figure 3(*c*). The calculated average diameter of grown MoO_3 MSs using software (Image J) is 0.8 μm with a standard deviation of 0.2 μm. These values were estimated making measurements on 15 MSs. A carefully examined SEM image at high magnification revealed that every MS is packed with vertically aligned nanoflakes with a mean thickness of nearly 60 nm (see the inset in figure 3(*d*)). These flakes attached on the surface of the spheres are not individual but in the form of self-assembled bunches aligned in parallel. It is believed that these bunches of nanoflakes are organized when more than one parallel flake is in close proximity, they tend to lean on each other and may be due to strong surface interactions [23], as can be seen in the inset of figure 3(*d*). These bunches are arrayed in all possible directions on the spherical surface, which is in complete agreement with the XRD findings. It is depicted from the micrograph that the parallel bunches of nanoflakes are not only growing on the curved surface of MSs but also on the neighbouring sites of MSs. The MoO_3 MSs attained a better spherical shape during the last deposition step than the previous one because the deposition in the final step is processed at high growth temperature (500 °C) using the PAS process. High growth temperature supplies additional thermal energy which allows the high mobility of incoming MoO_3 molecules migrating on the substrate to achieve the minimum energy configuration, as a result the well spherical shaped morphology is cropped out. It is to be noted that when the deposition of MoO_3 carried out on thermally evaporated MoO_3 film on Ni-coated glass by the PAS process in the case of the S–T sample, vertically aligned nanoplates are formed rather than spheres, as can be seen in figure 3(*a*). Therefore, it can be concluded that only S–T–S is the three-step optimum deposition sequence for the growth of MSs rather than the others. The structural and morphological studies confirmed that the fabrication of uniformly distributed α-MoO_3 MSs on the entire substrate offers very large reactive surface area, which may be a better candidate for applications such as secondary Li^+-ion batteries and gas sensor devices. We could not analyse the grown MSs accompanied with flakes in the S–T–S sample using TEM owing to the relatively large diameter of the spheres. These bunches of flakes detached from the MS surface when they disperse to ethanol with prolonged ultrasonication, permitting us to examine these flakes individually. As tested, the inter bonding among the nanoflakes is relatively strong, which was attributed to the lesser degree of disintegration in individual flakes of the nanoflake bunches. The low magnified bright field TEM micrograph of flakes is shown in figure 4(*a*); the dark portion in the TEM image indicates the bunching of nanoflakes with dense and smooth surfaces, which is very consistent with SEM results. A typical TEM image of well-shaped individual flakes is shown in figure 4(*b*), with the highlighted region for HRTEM analysis. Further characterization of MoO_3 nanoflakes is performed by HRTEM with a SAED pattern and divulged that nanoflakes existing on MSs are single crystalline with the top/bottom surface of [0 1 0] and the growth lying preferentially along the [0 2 1] direction. The SAED pattern of the S–T–S sample is obtained by focusing the electron beam normally to the anisotropic growth axis of a single flake is attributed to the [0 1 0] zone axis diffraction revealed in figure 4(*c*), which clearly exhibits diffraction spots with the *d*-spacing that could be indexed according to α-MoO_3 and indicates that the well crystallized single crystal nanoflakes are preferentially grown along the [0 2 1] direction on MSs. Figure 4(*d*) displays a typical fringe pattern taken from single nanoflakes from the highlighted region of the same sample. Parallel lattice fringes with a spacing of 0.327 nm corresponding to (0 2 1) crystal planes can easily be detected and agrees with the calculated spacing from XRD patterns.

Figure 5 shows the micro-Raman spectrum of the S–T–S sample to investigate the vibrational properties. The Raman spectrum of the S–T–S sample shows that sharp and intense peaks contribute to the good degree of crystallinity. The Raman peaks located at 275, 330, 369, 657, 811 and 987 cm^{-1} correspond to the α-MoO_3 crystal phase [24]. Vibrational analysis reveals that the peaks positioned in the 900–600 cm^{-1} and 400–200 cm^{-1} regions are due to the Mo–O stretching and bending modes, respectively. The absorption peaks at 987, 811 and 657 cm^{-1} in MoO_3 MSs are the characteristics of α-MoO_3. Generally, the orthorhombic α-MoO_3 crystalline structure can be visualized as consisting of corner-sharing chains of MoO_6 octahedra, in which one oxygen atom is unshared, two oxygen atoms are common with two octahedra and three oxygen atoms are in part-shared edges and common to three octahedra [25]. The narrow intense peak at 987 cm^{-1} is basically assigned to the terminal oxygen ($Mo^{6+} = O$) stretching mode along *a* and

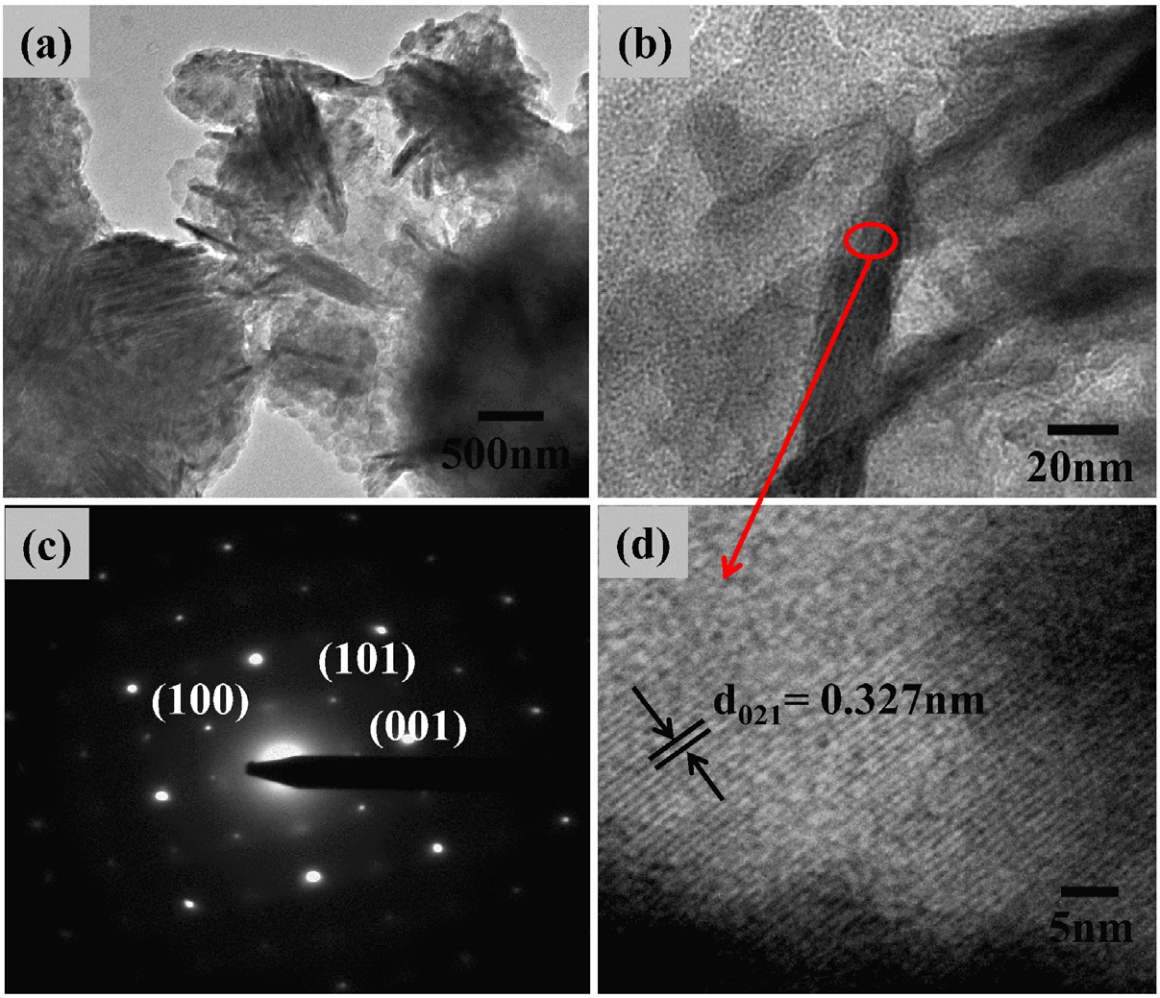

Figure 4. (*a*) Bright field TEM image of bunches of MoO_3 nanoflakes at low magnification; (*b*) TEM image of a single nanoflake with the highlighted region; (*c*) SAED pattern recorded for a single flake; (*d*) typical HRTEM image of an individual nanoflake with a fringe pattern.

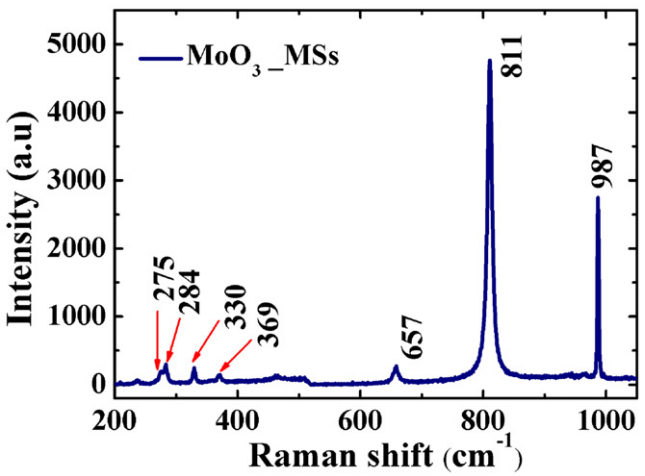

Figure 5. Micro-Raman spectrum of MoO_3 MSs for sample (S–T–S).

b directions, which results from unshared oxygen and is also responsible for the layered structure of α-MoO_3 [26]. The bridging oxygen atoms along the *c*-axis are weakly bound. The generation of oxygen vacancies should therefore lead to anion vacancies along the *c*-axis. Hence, the displacement of the Mo atom towards terminal oxygen in the *b*-axis can be expected upon loss of bridging oxygen, thus weakening the bond to the terminal O atom along the *a*-axis [27]. The intense Raman peaks at 811 cm^{-1} are attributed to the doubly coordinated oxygen (Mo_2–O) stretching mode, which results from corner-shared oxygen in common with two octahedra (alternating bond lengths of MoO_6). The peak at 657 cm^{-1} is assigned to the triply coordinated oxygen (Mo_3–O) stretching mode which results from edge-shared oxygen in common with three octahedra. The Raman peaks at 275 cm^{-1}, 330 cm^{-1} and 369 cm^{-1} can be specified to O–Mo–O scissoring and O=Mo=O wagging modes, respectively [28, 29]. The results obtained from Raman analysis are in good agreement with the conclusions drawn from x-ray analysis.

FTIR spectra are also recorded to investigate the chemical bonding states between molybdenum and oxygen atoms of the S–T–S sample in the range of 400–2000 cm^{-1} and can be seen in figure 6. The measured IR reflectance spectrum of MoO_3 MSs (in sample S–T–S) show several significant absorption peaks positioned at 1125, 988, 884, 827, 618 and 460 cm^{-1}. The analysis is based on the fact that MoO_3 is formed by MoO_6 octahedra for which stretching and bending

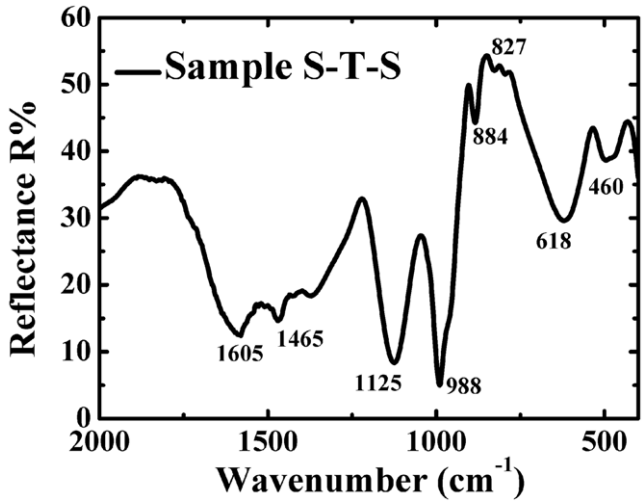

Figure 6. FTIR spectra of finally grown MoO_3 MSs packed with nanoflakes (sample S–T–S).

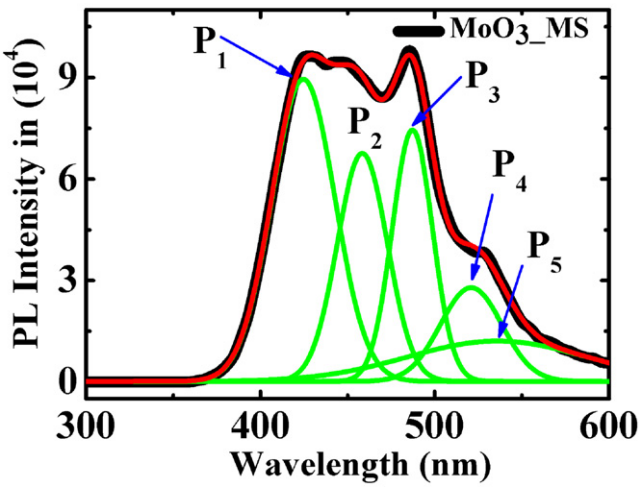

Figure 7. Gaussian convoluted form of PL spectra of MoO_3 MSs with peaks labelled as P_1, P_2, P_3, P_4, and P_5.

vibrational infrared active modes are invariably found in the range of 500–1200 cm^{-1} [30]. Two strong vibrations located at 884 and 988 cm^{-1}, associated with the symmetric stretching mode of oxygen in the Mo–O–Mo units and the Mo=O stretching mode. The absorption peak at 988 cm^{-1} represents the existence of terminal double bonds and confirms the basic characteristic of a layered structure of α-MoO_3. The weak absorption peak located at 827 cm^{-1} is attributed to the stretching mode of vibration of asymmetric bridging oxygen in Mo–O–Mo [31]. The band located in the range of 600–630 cm^{-1} shows typical vibration of the Mo_2O_2 entity formed by edge-shared MoO_6 polyhedra building the orthorhombic MoO_3 structure [30]. The peak at 778 cm^{-1} is due to the stretching mode of triply coordinated bridge-oxygen, caused by edge-shared oxygen atoms in common to three octahedrons. The peak presence at 460 cm^{-1} is due to the bending mode of the Mo–O–Mo entity [27]. In the present investigation, the presence of absorption peaks positioned at 1465 and 1605 cm^{-1} correspond to a bending mode of Mo–OH bonds [31]. In addition, the absorption peak positioned at 1125 cm^{-1} also evidences the presence of water content on the film surface.

PL emission spectrum of the S–T–S sample is measured in the wavelength range from 300 to 600 nm and the excitation wavelength is 250 nm (4.95 eV) more than the band gap energy. The broad hump in the PL spectrum is the signature of the size distribution of MSs with improved crystallinity and confirmed with the SEM and XRD analysis. The deconvoluted PL emission spectrum of the S–T–S sample is depicted in figure 7. The MSs exhibit PL emission peaks positioned at the wavelengths 424, 457 nm, 486 nm, 521 nm and 536 nm, labelled as P_1, P_2, P_3, P_4, and P_5, respectively. These luminescence peaks of molybdenum oxide MSs may be attributed to radiative decay of self-trapped excition, linked to some lattice defects like oxygen vacancies, the other complex defect centres such as the clustering of oxygen vacancies, and the lower valence Mo^{5+} ion associated with the transfer of charge from oxygen vacancies to Mo ions [32, 33]. As shown in the picture, luminescence peak P_1 positioned at 424 nm ascribed the transition close to the near band edge emission, which is assigned to the free excition recombination also in accordance with the earlier reported results [34]. The transitions located at 457, 486, 527 and 536 nm may be attributed, in the crystal field model, to the Mo^{5+} d–d band transition of a heavily distorted polyhedron (Mo–O) in an octahedral crystal field [24, 35]. The band at 2.71 (457 nm) and 2.55 eV (486 nm) in the emission spectrum can be attributed to the deep level $Mo^{5+} d^2_{yz} - d^2_{xz}$ transition [35]. It is reported that the MoO_3 film grown by TE at room temperature is rich in defects, like oxygen vacancies [36], therefore the observed prominent PL emission peaks due to the defects, especially from oxygen vacancies, may arise from the intermediate layer grown during the second deposition step. In addition, the PL spectrum of MoO_3 MSs reveals the band-to-band transition at 424 nm (2.90 eV), which is rather smaller than the value of 3.15 eV of bulk MoO_3 [37], which demonstrates the nanosize effect on electronic spectra. It has been reported earlier that the oxygen vacancies of MoO_3 will lead to a red-shift phenomenon. Sian and Reddy [36] found that the oxygen vacancies could generate a defect band above the valance band of MoO_3, resulting in the band gap reduction. In our case, the existence of oxygen vacancies is confirmed by the PL spectrum itself as well as the Raman spectrum.

For both scientific understanding and novel applications, it is necessary to study the growth mechanism of MoO_3 MSs. In order to understand the growth of MoO_3 MSs packed with nanoflakes, the surface morphologies of films formed at the different deposition stages are collected for SEM measurement, as shown in figures 2 and 3. The schematic diagram of the growth mechanism is illustrated in figure 8 in three consecutive stages. At the initial deposition step (in stage I), vertically aligned nanoflakes are formed on the nickel-coated substrate by the PAS process (see figure 8(*b*)). It is observed that the cracking arises on the nickel film owing to the difference in the thermal expansion coefficients, facilitating the growth of α-MoO_3 nanoflakes, which functioned as a primary seed layer for further growth. These flakes are different in terms of height because some flakes are tilted at a certain angle due to the formation of multipod-like junctions. The

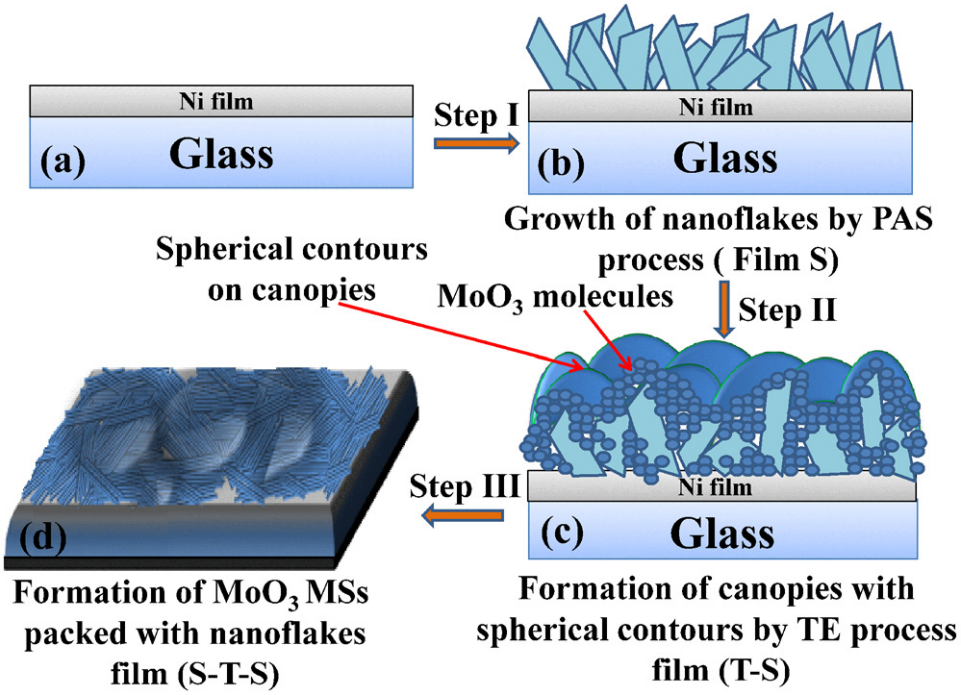

Figure 8. Schematic representation of the proposed growth model in three steps to grow MoO_3 MSs packed with self-assembled nanoflakes.

existence of defects, like oxygen vacancies in the MoO_3 films, can increase the possibility of forming multipod-like junctions (see the inset of figure 2(*b*)), resulting in enhanced surface roughness due to tilted nanoflakes [38]. The second deposition stage basically includes the deposition of MoO_3 by TE on pre-deposited nanoflakes at room temperature. At this growth stage, canopies with spherical contours of variable radii are formed. The curvature of contours in canopies is guided by the topology of the bottom layer. On the other hand, in this growth stage the coming MoO_3 vapour during TE starts to condense on the fine edges of the flakes, but because of large surface roughness, the uniform smooth film does not form. The incoming MoO_3 molecules start to sit preferentially on the uppermost part of the film and with the filling of voids existing among the nanoflakes, as can be seen in figure 8(*c*), eventually the spherical contours of different radii of curvatures are cropped out (see figure 2(*c*)). Since during the thermal evaporation of MoO_3 substrate is placed at room temperature, as a result the incoming MoO_3 molecules have no additional thermal energy on the substrate to enhance their mobility to migrate on the substrate surface, which also promotes the formation of spherical contours on canopies. It is reported that MoO_3 have excellent spreading ability, which facilitates the maintenance of the uniformity on the entire substrate area during the second deposition stage [39]. The morphological results divulged that the presence of both the vertical nanoflakes in the primary seed layer as well as the spherical contours on the intermediate film are crucial for the growth of MoO_3 MSs. As reported earlier, the film deposited at room temperature by the TE process may be rich in defects, like oxygen vacancies relative to the film deposited by the PAS process at high growth temperature [36]. The bluish colour of the intermediate film can be assumed as proof of the existence of oxygen vacancies. The final step includes the deposition of MoO_3 by the PAS process on the same substrate by keeping the processing parameters fixed the same as in the first deposition step. It is believed that there are two processes: one is the coalescence of contours and the other is the deposition of MoO_3 by sublimation taking place simultaneously during final growth. The high growth temperature not only assists with the growth of well-shaped nanoflakes on MSs, but also in the coalescence of contours (which is the core of MSs) to acquire a more spherical shape by minimizing their surface energy. It is mentioned above that the intermediate layer acts as a reactive surface for the further coming MoO_3 molecules and the nucleation of MoO_3 molecules on the surface depends strongly on the amount of active oxygen [40]. The oxygen vacancies on the canopies provide the nucleation sites for further growth and strongly lower the barrier for the incorporation of coming vapour on the substrate. It is supposed that high substrate temperature in final growth supplies additional thermal energy, which offers the high mobility of MoO_3 molecules to migrate onto the substrate for accomplishing the preferential heterogeneous nucleation sites as well as the high coalescence rate of the contours. As a result, a large number of nuclei are formed on the intermediate layer, which begin to coalesce and form the continuous larger grains in the shape of nanoflakes. Since the MoO_3 grains have a larger diffusion coefficient. This enhanced rearrangement with high growth temperature and the gradual formation of MSs packed with nanoflakes can be seen in figure 8(*d*). It is worthwhile to note that the curvature of canopies is significantly increased at high growth temperature, which made the contours more spherical on canopies, as previously. Also the presence of the temperature gradient between the uppermost film and the base of the substrate will

enhance the surface mobility of atoms and may favour the upper growth of nanoflakes located on the surface of MSs during the growth process. The flakes being on MSs are not individual but in the form of bunches aligned in parallel, which may be because of strong Colombian surface interactions. It is reasonable to expect that the orientation of nanoflake bunches on MoO_3 MSs is also modified by the existence of oxygen vacancies on canopies.

4. Conclusions

Molybdenum oxide MSs packed with vertically aligned nanoflakes (sample S–T–S) are successfully synthesized by plasma-assisted sublimation (PAS) and thermal evaporation (TE) processes in three consecutive steps. The investigations reveal that the intermediate layer formed in the second deposition step is crucial for the formation of MSs. The morphological and structural studies of the S–T–S sample confirmed the uniform growth of MSs with nanoflakes on large area scale, having a single orthorhombic phase. The flakes embedded on the surface of the spheres are in the form of randomly aligned bunches, which may be because of some surface interactions. Further investigations of MoO_3 MSs are carried out by HRTEM with SAED, which endorsed the single crystalline nature of nanoflakes lying on the surface of MSs. The vibrational study of MSs is accomplished by FTIR and micro-Raman measurements and supports the XRD findings. The MoO_3 microspheres show that the room temperature PL with a broad hump is the signature of the size distribution of microspheres. The ability to produce the molybdenum oxide MSs packed with nanoflakes in thin films with reproducible structural, morphological and optical characteristics should be useful for the application of gas sensing and highly efficient lithium ion batteries.

Acknowledgments

One of the authors Rabindar K Sharma gratefully acknowledges financial assistance from the Council of Scientific and Industrial Research (CSIR)-India.

References

[1] Ewers T D, Sra A K, Norris B C, Cable R E, Cheng C H, Shantz D F and Schaak R E 2005 *Chem. Mater.* **17** 514
[2] Mo M, Yu J C, Zhang L Z and Li S K A 2005 *Adv. Mater.* **17** 756
[3] Liu L, Li Y, Yuan S M, Ge M, Ren M M, Sun C S and Zhou Z 2010 *J. Phys. Chem.* C **114** 251
[4] Abello S, Medina F, Tichit D, Pérez-Ramírez J, Cesteros Y, Salagre P and Sueiras J E 2005 *Chem. Commun.* 1453
[5] Hu L, Zhong H, Zheng X, Huang Y, Zhang P and Chen Q 2012 *Sci. Rep.* **2** 986
[6] Li X, Si Z, Lei Y, Tang J, Song S and Zhang H 2011 *Cryst. Eng. Commun.* **13** 642
[7] Sian T S and Reddy G B 2005 *J. Appl. Phys.* **98** 026104
[8] Taurino A M, Forleo A, Francioso L and Siciliano P 2006 *Appl. Phys. Lett.* **88** 152111
[9] Liu C, Li Z and Zhang Z 2011 *Appl. Phys. Lett.* **99** 223104
[10] Zhou J, Deng S Z, Xu N S, Chen J and She J C 2003 *Appl. Phys. Lett.* **83** 2653
[11] Diaz-Droguett D E, Fuenzalida V M and Solorzano G 2008 *J. Nanosci. Nanotechnol.* **8** 5977
[12] Yan B, Zheng Z, Zhang J, Gong H, Shen Z, Huang W and Yu T 2009 *J. Phys. Chem.* C **113** 20259
[13] Khademi A, Azimirad R, Zavarian A A and Moshfegh A Z 2009 *J. Phys. Chem.* C **113** 19298
[14] Zakharova G S, Taschner C, Volkov V L, Hellmann I, Klingeler R, Leonhardt A and Buchner B 2007 *Solid State Sci.* **9** 1028
[15] Song R Q, Xu A W, Deng B, Fang Y P 2005 *J. Phys. Chem.* B **109** 22758
[16] Liu J, Sasidharan M, Liu D, Yokoyama Y, Yusa S-i and Nakashima K 2012 *Mater. Lett.* **66** 25
[17] Fei J, Cui Y, Yan X, Qi W, Yang Y, Wang K, He Q and Li J 2008 *Adv. Mater.* **20** 452
[18] Guo S, Wang L and Wang E 2007 *Chem. Commun.* 3163
[19] Cao F, Hu W, Zhou L, Shi W, Song S, Lei Y, Wang S and Zhang H 2009 *Dalton Trans.* 9246
[20] Li Y, Liu J, Huang X and Li G 2007 *Cryst. Growth Des.* **7** 1350
[21] Siciliano T, Tapore A, Filippo E, Micocci G and Tepore M 2009 *Mater. Chem. Phys.* **114** 687
[22] Sharma R K and Reddy G B 2013 *AIP Adv.* **3** 092112
[23] Li Y, Liu J, Xintang H and Li G 2007 *Cryst. Growth Des.* **7** 7
[24] Dieterle M and Mesti G 2002 *Phys. Chem. Chem. Phys.* **4** 822
[25] Anderson G and Magneli A 1950 *Acta Chem. Scand.* **4** 793
[26] Beattie I R and Gilson T R 1969 *J. Chem. Soc.* A 2322
[27] Mestl G, Verbruggen N F D, Bosch E and Knozinger H 1996 *Langmuir* **12** 2961
[28] Py M A and Maschke K 1981 *Physica* B **105** 370
[29] Klinbumrung A, Thongtem T and Thongtem S 2012 *J. Nanomater.* **1** 1155
[30] Rao K S, Kanth B R and Mukhopadhyay P K 2009 *Appl. Phys.* A **96** 985
[31] Sain T S and Reddy G B 2004 *Appl. Surf. Sci.* **236** 1
[32] Itoh M, Hayakawa K and Oishi S 2001 *J. Phys.: Condens. Matter* **13** 6853
[33] Zhoa Y, Liu J, Zhou Y, Zhang Z, Xu Y, Naramoto H and Yamamoto S J 2003 *J. Phys.: Condens. Matter* **15** L547
[34] Song J, Ni X, Zhang D and Zheng H 2006 *Solid State Sci.* **8** 1164
[35] Labanowaka M 1999 *Phys. Chem. Chem. Phys.* **1** 5385
[36] Sian T S and Reddy G B 2004 *Sol. Energy Mater. Sol. Cells* **82** 375
[37] Erre R, Legay M H and Fropiat J J 1983 *Surf. Sci.* **127** 69
[38] Fuller M L 1944 *J. Appl. Phys.* **15** 164
[39] Song Z, Cai T, Chang Z, Liu G, Rodriquez J A and Hrbek J 2003 *J. Am. Chem. Soc.* **125** 8059
[40] Liu X, Wu X, Cao H and Chang R P H 2004 *J. Appl. Phys.* **95** 3141